Electronic Supplementary Material (ESI) for Inorganic Chemistry Frontiers.

Zirconium-based metal-organic frameworks: The relation between linker connectivity, structure stability, and catalytic activity towards organophosphates

Daniel Bůžek,*[a,b] Jan Hynek,[a] Matouš Kloda,[a] Veronika Zlámalová,[b] Petr Bezdička,[a] Slavomír Adamec,[b] Kamil Lang,[a] Jan Demel[a]

[a]Institute of Inorganic Chemistry of the Czech Academy of Sciences, 250 68 Husinec-Řež č.p. 1001, Czech Republic. E-mail: buzek@iic.cas.cz

[b]Faculty of Environment, Jan Evangelista Purkyně University in Ústí nad Labem, Pasteurova 3632/15, 400 96 Ústí nad Labem, Czech Republic

Electronic Supplementary Information

Content

Table S1 List of used chemicals

Compound	Quality	Producer
Acetic anhydride	ACS reagent, ≥98.0%	Sigma-Aldrich
Acetic acid	99%	Penta Chemicals
Aceton	p. a.	Penta Chemicals
Acetonitrile	Chromasolv, for HPLC, gradient grade	Honeywell
Ammonium cerium(IV) nitrate	≥99.99% trace metals basis	Sigma-Aldrich
N,N-Dimethylformamide (DMF)	p. a.	Penta Chemicals
Formic acid	98%	Penta Chemicals
Hafnium chloride	98%	Sigma-Aldrich
Methanol (for MOF cleaning)	p. a.	Penta Chemicals
Methanol (for HPLC)	Chromasolv, for HPLC, gradient grade	Honeywell
5,5′- Methylenediisophtalic acid (H_4MDIP)	98%	BLDpharm
Sodium hydroxide	p. a.	Lach:ner
Terephthalic acid (H_2BDC)	98%	Sigma-Aldrich
Trimesic acid (H_3BTC)	98.3%	BLDpharm
Zirconium chloride	≥99.5%	Sigma-Aldrich
Zirconyl chloride octahydrate	Reagent grade, 98%	Sigma-Aldrich
4-Formylbenzoic acid	99.1%	BLDpharm
Pyrrole	99%	Fluorochem
Propionic acid	99.99%	Lach:ner
Dichloromethane	p. a.	Lach:ner
Methyl paraoxon (DMNP)	Pestenal, analytical standard	Sigma-Aldrich
4-Nitrophenol (4-NP)	Spectrophotometric grade	Sigma-Aldrich
Zinc oxide	ACS, p. a.	Roth
Tetrahydrofurane (THF)	p. a.	Penta Chemicals
Ethanol (EtOH)	Absolute	Penta Chemicals
Orthophosphoric acid	85%	Lach:ner
Hydrochloric acid	35%+, p. a.	Penta Chemicals
Nitric acid	65%, p. a.	Lach:ner
Hydrofluoric acid	38-40%, p. a.	Lach:ner
Indium solution	CRM, Solution 100 mg L^{-1}	Astasol (Analytika s.r.o.)
DMSO-d6	99.8%	Eurisotop
Zirconium standard ICP	CRM, mixture of 18 elements, 100 mg L^{-1}	Astasol (Analytika s.r.o.)

Synthesis of materials

Zr-based UiO-66 was synthesized by a modified procedure published previously.[1,2] First, a stock solution of reactants was prepared by the dissolution of 2.12 g (9.09 mmol) $ZrCl_4$ in 400 mL of DMF upon 30 min of sonication followed by the addition of 1.51 g (9.09 mmol) H_2BDC and additional 10 min of sonication. Then, the solution was divided into 20 mL portions and transferred to 40 mL Wheaton vials. After that, 2.5 mL of acetic acid (modulator) was added to each vial. The reaction mixture in the sealed vials was placed into a preheated oven (Memmert UF110plus) and kept at 120 °C for 24 h. After cooling down, the white precipitate was collected by centrifugation (4000 rpm, Hermle ZK 496) and washed four times with DMF (25 mL per each cycle) and five times with acetone (25 mL per each cycle). The use of water for washing was avoided to prevent potential hydrolytic reactions. The product was air-dried for 24 h and vacuum-dried at 120 °C for additional 24 h.

Hf-based UiO-66 (UiO-66(Hf)) was prepared in the same way as Zr-based UiO-66 using 2.91 g (9.09 mmol) of $HfCl_4$ instead of $ZrCl_4$.

Ce-based UiO-66 (UiO-66(Ce)) was prepared using a previously published procedure[3] in a 50 times larger scale: 1.78 g (10.7 mmol) of H_2BDC was dissolved in 60 mL of DMF, and separately 5.84 g (10.7 mmol) of ($Ce(NH_4)_2(NO_3)_6$) was dissolved in 20 mL of water. The H_2BDC solution was heated in an oil bath to 100 °C, then the $Ce(NH_4)_2(NO_3)_6$ solution was added upon mild stirring, and the reaction flask was sealed. The crystallization under stirring occurred within 20 min at 100 °C. The product was separated and washed in the same way as in the case of the Zr-based UiO-66.

MOF-808 was prepared according to a published optimized procedure[4] leading to a well crystalline powder in a 16 times larger scale. The stock solution of $ZrCl_4$ was prepared by dissolving 16.8 g (72.1 mmol) $ZrCl_4$ in 480 mL of acetic acid. The stock solution of H_3BTC was prepared by dissolving 4.96 g (23.6 mol) H_3BTC in 480 mL of DMF. The reaction mixtures were prepared by mixing 30 mL of $ZrCl_4$ stock solution with 30 mL of H_3BTC solution in DURAN glass bottles, which were then sealed and heated in a preheated oven at 120 °C for 72 h. The product separation, washing, and activation were performed analogously to UiO-66.

MIP-200 was synthesized according to a published procedure[5] modified to achieve the phase purity with a good reproducibility. First, 12.5 mL of formic acid and 17.5 mL of acetic anhydride were mixed. A DURAN glass bottle was charged with 212.5 mg (0.615 mmol) of H_4MDIP and 30 mL of the prepared solution was added. The yellow suspension was sonicated for 30 min at constant temperature of 30 °C. The compound did not fully dissolve at this temperature and the reaction mixture formed a suspension. After the sonication, 430 mg (1.845 mmol) of $ZrCl_4$ was added upon stirring. The reaction vessel was sealed and stirred for 20 min. Then, the magnetic stirring bar was removed and the reaction mixture was placed into a preheated oven and kept at 120 °C for 72 h. The product was collected by centrifugation (4000 rpm, Hermle ZK 496) and washed once with EtOH (25 mL) and five times with MeOH (25 mL per each cycle). The reported washing procedure involves water,[5] however, we decided to skip this step to avoid potential hydrolytic processes in the MOF. MIP-200 was dried in the same way as UiO-66.

Before the synthesis of PCN-222, the linker **5,10,15,20-tetrakis(4-carboxyphenyl)porphyrin (H_4TCPP)** was prepared by the standard porphyrin synthesis.[6] A 1L round-bottom flask was charged with 21.64 g (144 mmol) of 4-formylbenzoic acid and 500 mL of propionic acid. The mixture was heated

to 140 °C and 10 mL (144 mmol) of pyrrole was added. After 4 h of stirring, the reaction mixture was cooled down to RT, the formed precipitate was collected by vacuum filtration, thoroughly washed with methanol, dichloromethane and hot water, and vacuum-dried.

Yield: 7.95 g (28 %).

^{1}H NMR (DMSO-d_6): δ 8.81 (s, 8H), 8.35 (d, $^{3}J_{HH}$ = 7.9 Hz, 8H), 8.30 (d, $^{3}J_{HH}$ = 7.9 Hz, 8H), -2.98 (s, 2H).

PCN-222 was synthesized by a modified procedure described earlier,[7] based on the work of Morris *et al*.[8] In short, 300 mg (0.931 mmol) of zirconyl chloride octahydrate was dissolved in 80 mL of DMF followed by 30 min of sonication. Next, 233 mg (0.295 mmol) of H_4TCPP was added to the solution and sonicated again for 10 min. The solution was transferred to a Teflon lined autoclave (Berghof DAB-3) and 40 mL of formic acid was added. The autoclave was sealed and inserted in the preheated oven at 130°C for 72 h. After the crystallization, the solid was washed using procedure described for UiO-66, air-dried and activated in the same way as UiO-66.

Instruments and measurement conditions

X-ray powder diffraction (XRPD) patterns were collected using a PANalytical X´Pert PRO diffractometer equipped with a conventional X-ray tube (Cu K_α 40 kV, 30 mA, line focus) in the transmission mode. An elliptic focusing mirror, a divergence slit 0.5°, an anti-scatter slit 0.5°, and a Soller slit of 0.02 rad were used in the primary beam. A fast linear position sensitive detector PIXcel with an anti-scatter shield and a Soller slit of 0.02 rad were used in the diffracted beam. All patterns were collected in the range of 1 to 85° 2θ with the step of 0.013° and 300 s / step producing a scan of about 2.25 h. Samples were placed on the top of a mylar foil to a transmission sample holder. The thin layer of as prepared sample was then covered with the second mylar foil.

For estimating the amorphous content, we used the addition of an internal standard - ZnO (Roth p.a. ACS, calcined to 700 °C for 5 h). The MOF sample was mixed with 50 wt% of ZnO and approximately 5 mL of acetone was added. The resulting mixture was mixed for 10 min in an agate mortar to make a homogeneous mixture. The prepared samples were analysed by XRPD in the conventional Bragg – Brentano reflection geometry with top-loaded sample holders using a PANalytical X´Pert PRO diffractometer equipped with a conventional X-ray tube (Cu K_α radiation, 40 kV, 30 mA) and a linear position sensitive detector PIXcel with an anti-scatter shield. A programmable divergence slit set to a fixed value of 0.125°, Soller slit of 0.02 rad, and mask of 15 mm were used in the primary beam. A programmable anti-scatter slit set to a fixed value of 0.125°, Soller slit of 0.02 rad, and Ni beta-filter were used in the diffracted beam. The data were collected in the range of 1.5 – 85° 2θ with a step of 0.0131 ° and 400 s / step. The scan took approximately 3 h.

Evaluation of XRPD patterns. Qualitative analysis was performed with the HighScorePlus software package (Malvern PANalytical, The Netherlands, version 5.2.0)[9] together with the Crystallography Open Database (COD),[10] the Cambridge Structural Database (CSD),[11] and the PDF-5+ database.[12] For the quantitative phase analysis, based on the Rietveld method, the Profex 5.2.8 / BGMN 4.2.23 code was used.[13,14,15,16] The models of MOFs were taken from the COD database[10] (UiO-66 – 4512074) and the CSD database[11] (MOF 808 – BOHWUS, MIP-200 – IYUFUG). The model of ZnO was taken from the PDF-5+ database.[12]

The analyses of released linkers (measured as corresponding acids H_2BDC, H_3BTC, H_4MDIP, and H_4TCPP) were performed using a high-performance liquid chromatography (HPLC) instrument Agilent 1260 Infinity II, equipped with a diode array detector (DAD) fitted with an autosampler and a chromatographic column YMC Hydrosphere C18 (50 mm x 4.6, S-3 µm, 12 nm) used at constant temperature of 30 °C. An injected volume of the sample was 10 µL and the mobile phase was acidified by the addition of formic acid (0.1 vol.%), the exact ratios of mobile phase solvents are given in Table S2 for each linker. The flow rate was 0.5 mL min^{-1}. The amount of released linker was quantified using the calibration curves. The validation parameters of the HPLC analyses are also given in Table S2.

The analyses of monocarboxylic acids in dissolved MOFs, methyl paraoxon (DMNP), and 4-nitrophenol (4-NP) were performed by an HPLC-DAD DIONEX Ultimate 3000 instrument equipped with a DAD, manual sample injection with a 20 µL sampling loop and a thermostat to keep constant temperature of 30°C. The content of formic and acetic acid was analysed on a chromatographic column Phenomenex Synergy polar-RP (100 mm x 4.6 mm, 4 µm, 80 Å) using a mobile phase containing 0.05 M H_3PO_4.

Before each sample injection, the column was washed with a 40 / 60 vol.% 0.05 M H_3PO_4 / MeCN (or MeOH for the H_4TCPP samples) mixture to remove all residual organic linkers originating from the previous sample. The flow rate was adjusted to 0.5 mL min^{-1} and the detailed chromatographic parameters are summarized in Table S2. In the case of DMNP and 4-NP, the instrument was equipped with a Phenomenex Kinetex C18 (50 mm x 3 mm, 2.6 μm) column, and a water / methanol mixture in 40 / 60 vol.% ratio, both acidified with formic acid (0.1 vol.%), was used as a mobile phase. All chromatographic parameters are also included in Table S2.

Table S2 Mobile phases and selected validation parameters for HPLC analyses of given analytes.

Analyte	H_2O (vol.%)	MeCN (vol.%)	MeOH (vol.%)	THF (vol.%)	Detection wavelength (nm)	Time of analysis / retention time (min)	LOD[a] (mg L^{-1})	LOQ[b] (mg L^{-1})	Error of repeated analysis (RSD %)
H_2BDC (UiO-66)	75.0	25.0	0	0	242	3.4 / 2.5	0.01	0.05	< 7
H_3BTC (MOF-808)	77.5	22.5	0	0	214	3.0 / 2.3	0.005	0.01	< 6
H_4MDIP (MIP-200)	68.0	32.0	0	0	212	4.0 / 2.3	0.05	0.10	< 6
H_4TCPP (PCN-222)	12.5[c]	0	67.5[c]	20	416	4.0 / 2.8	0.005	0.01	< 4
HCOOH	100[d]	0	0	0	205	5.0 / 2.8	0.1	0.5	< 6
CH_3COOH	100[d]	0	0	0	205	5.0 / 3.4	0.5	1.5	< 8
DMNP	60[c]	0	40[c]	0	273	3.0 / 1.8	n. a.	n. a.	< 5
4-NP	60[c]	0	40[c]	0	316	3.0 / 1.4	n. a.	n. a.	< 5

[a] LOD = limit of detection, calculated as: LOD = 3 x noise, verified also by experiments.

[b] LOQ = limit of quantification, calculated as: LOQ = 10 x noise, verified by experiments.

[c] Acidified by adding 0.1 vol.% of HCOOH.

[d] Water with 0.05 M of H_3PO_4.

Zirconium content was determined by inductively coupled plasma mass spectrometry (ICP-MS) on an Agilent 7900 instrument equipped with an agon burner, an ORS 4 collision cell, and a mass analyser based on a hyperbolic quadrupole with an orthogonal detection system. Indium solution (100 ppb) was added as an internal standard for the recognition of the matrix influence. The content of zirconium was quantified using calibration curves. Before the analysis, the solid samples were dissolved by the following procedure: 10 mg was dissolved in a mixture of 12 mL HCl, 4 mL HNO_3, and 4 mL HF under microwave irradiation using an Anton Paar multiwave 5000 instrument and the resulting liquid sample was diluted with water to a final volume of 30 mL. Each sample was analysed at least twice.

Fourier transform infrared (FTIR) spectra were measured by a Thermo Nicolet NEXUS-FTIR 670 spectrometer equipped with an ATR probe. N_2 adsorption isotherms were recorded at 77 K using a 3P micro 300 instrument (3P Instruments). Prior to the measurements, the samples were degassed at 120 °C for 16 h under dynamic vacuum, and then additionally activated at 120 °C for 3 h using a turbomolecular pump. Only in the case of PCN-222, activation temperature was set to 80 °C.

Differential thermal analyses (TGA/DTA) were carried out using a Setaram SETSYS Evolution-16-MS coupled with a mass detector (MS) for the qualitative determination of emitted gases. The analyses were performed in the flow of synthetic air with a flow rate of 30 mL min^{-1} and within a temperature range from laboratory temperature (approximately 20 °C) to 800 °C with a heating rate of 5 °C min^{-1}.

Catalytical degradation of DMNP. For the catalytic experiments we used MOFs samples collected from time-dependent release experiments (240 min) at indicated pH. Before the catalytical experiments, 5 mg of an activated MOF was mixed with 1 mL of neat water followed by short sonication. Next, 1 mL of 2mM DMNP stock solution was added so that the initial concentration of DMNP was 1mM. Experiments were performed under constant temperature of 25 ± 1 °C and the mixture was stirred. Aliquots of 50 µL were taken at predefined times ranging from 2.5 to 240 min, mixed with 950 µL of extractive solution (60 % MeOH, 40 % H_2O, acidified with 0.1 % HCOOH), and filtered using 0.2 µm PTFE Whatman microfilters. Filtered samples were analysed by HPLC. All catalytical experiments were repeated at least twice. At the end of the experiments, we also measured pH which was in the range from 3.9 to 4.6 for all tested samples. Finally, we also monitored linker release from MOFs during the catalysis which was below the limit of detection in all cases, indicating that the MOFs are stable during the catalytic reaction. Blank experiment (without a MOF) showed only negligible hydrolysis of DMNP under given conditions.

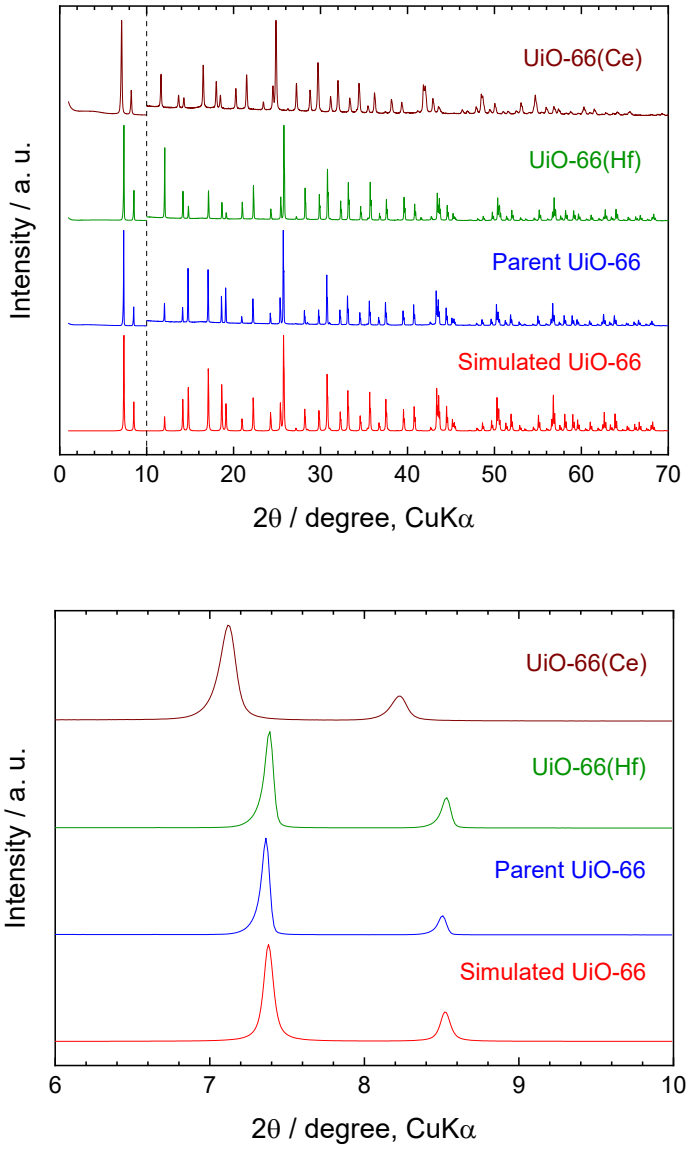

Figure S1 Top panel: XRPD patterns of UiO-66 (labelled as parent UiO-66, UiO-66(Ce), and UiO-66(Hf)) compared with those calculated from the corresponding CIF (labelled as simulated UiO-66).[17] Diffractograms are normalized and shifted vertically to avoid overlaps. The diffractograms are zoomed from 10° 2θ to visualize diffractions at higher angles. Bottom panel: all diffractograms between 6° and 10° 2θ for visualization of the broadening of the first two diffraction lines. The integral breadth (IB) was calculated by the line profile analysis procedure with the Voigt function (split width) using the HighScorePlus software.[9] The calculated IB of the first two diffraction lines were 0.083 and 0.079 ° 2θ for parent UiO-66, 0.092 and 0.089° 2θ for UiO-66(Hf), and 0.168 and 0.162 ° 2θ for UiO-66(Ce). These observations indicate that UiO-66 and UiO-66(Hf) have comparable sizes of crystallites, whereas the crystallite size of UiO-66(Ce) is lower. To be more specific, applying the instrumental IB obtained using the SRM660a (LaB_6) standard and extrapolated to the appropriate angular region, the estimated crystallite sizes are 310, 225, and 70 nm for parent UiO-66, UiO-66(Hf), and UiO-66(Ce), respectively.

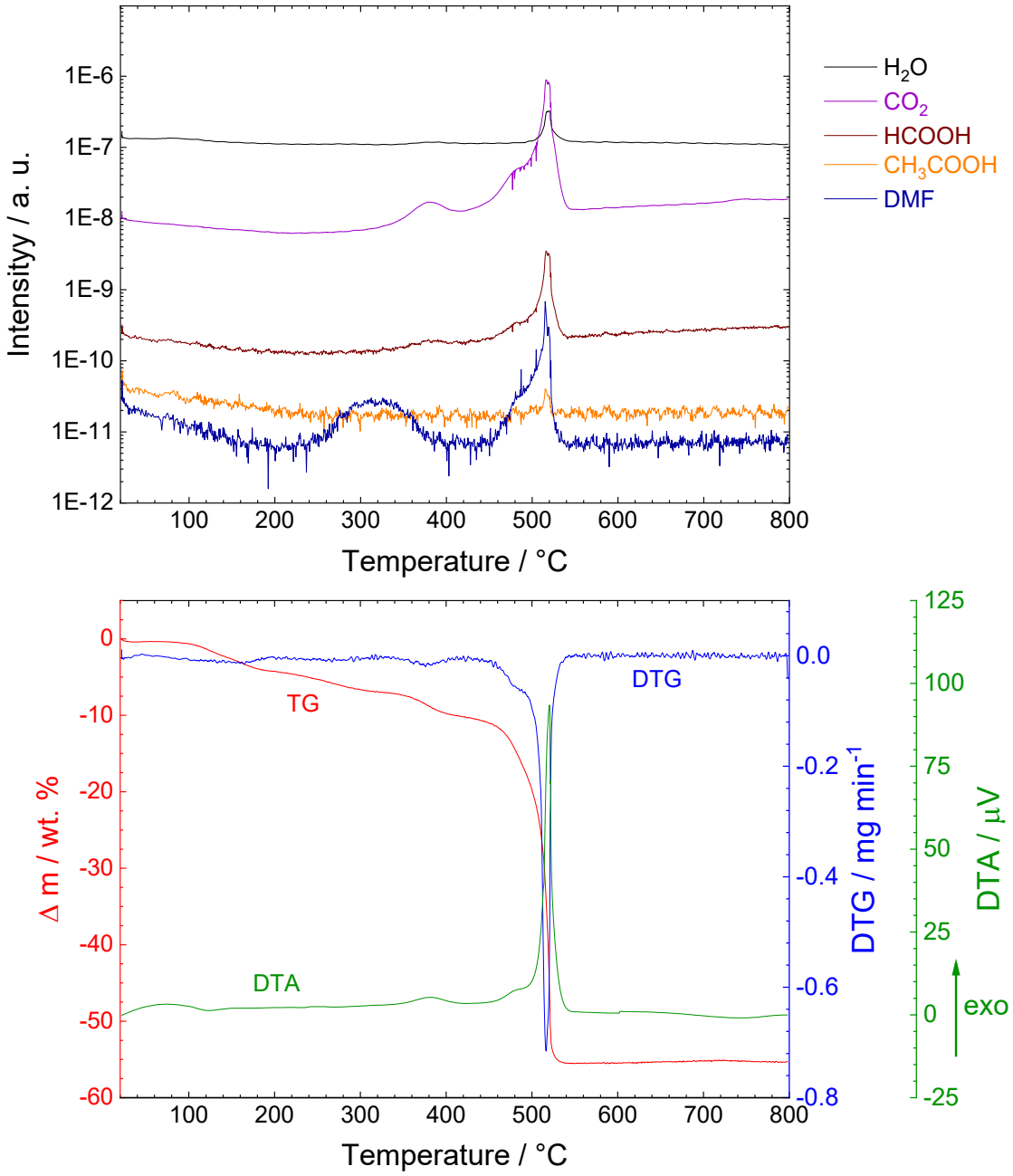

Figure S2 TGA/DTA curves of the parent Zr-based UiO-66 (bottom) and MS analysis of the gases evolved during the TGA/DTA measurement (top).

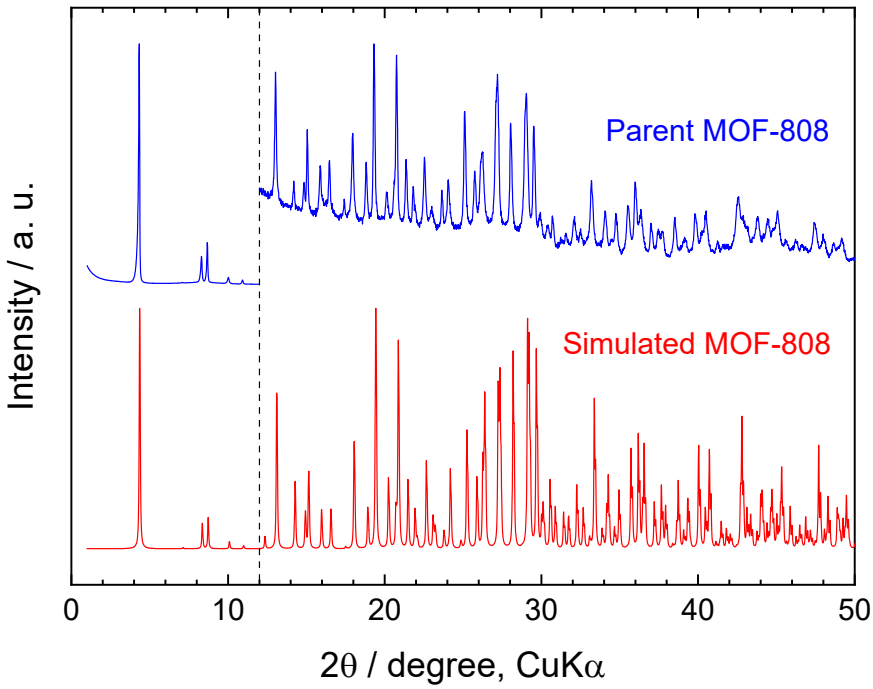

Figure S3 XRPD pattern of the parent MOF-808 compared with that calculated from the corresponding CIF file (labelled as simulated MOF-808).[18] Diffractograms are normalized and shifted vertically to avoid overlaps. The diffractograms are zoomed from 12° 2θ to visualize diffractions at higher angles.

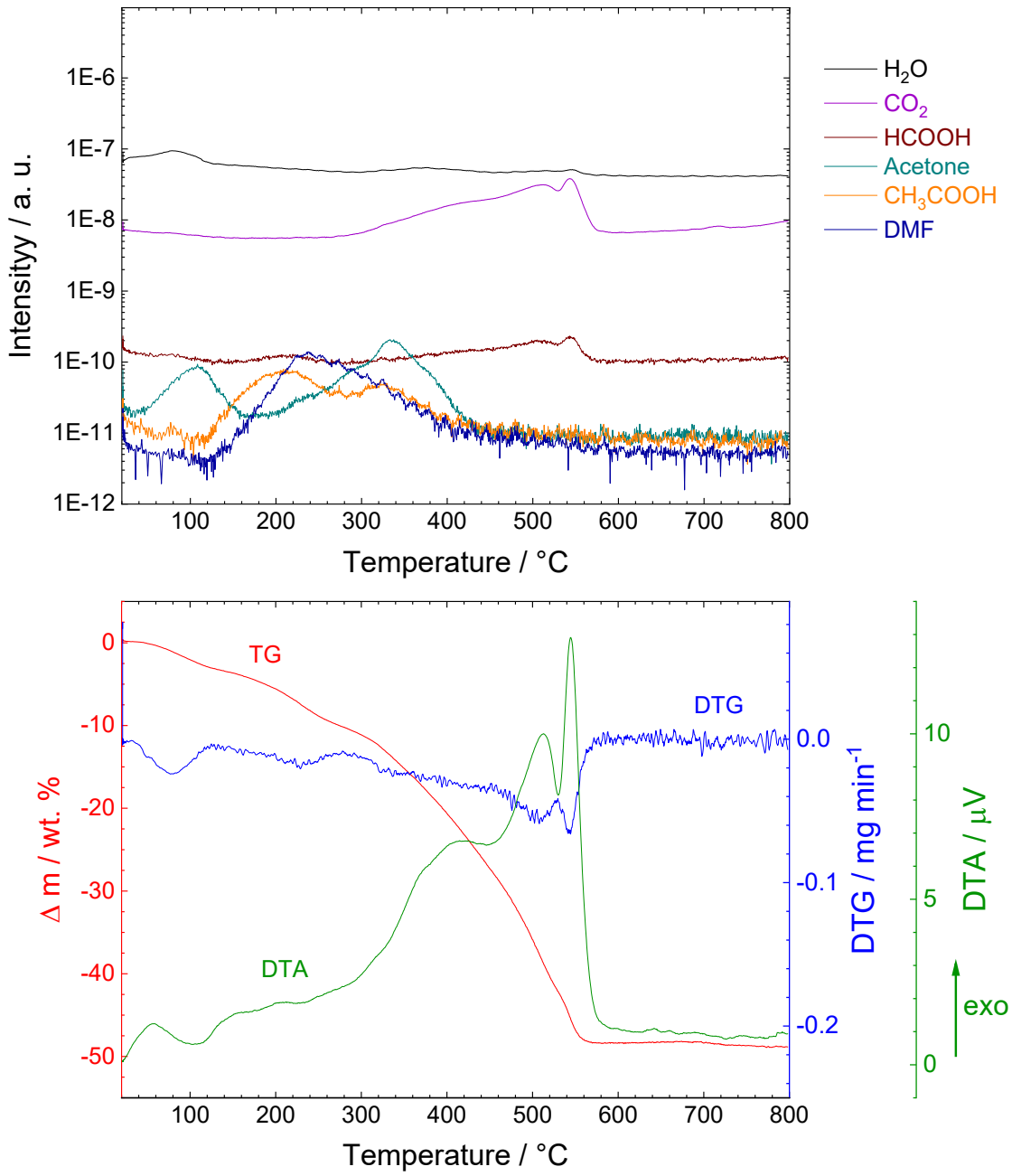

Figure S4 TGA/DTA curves of the parent MOF-808 (bottom) and MS analysis of the gases evolved during the TGA/DTA measurement (top).

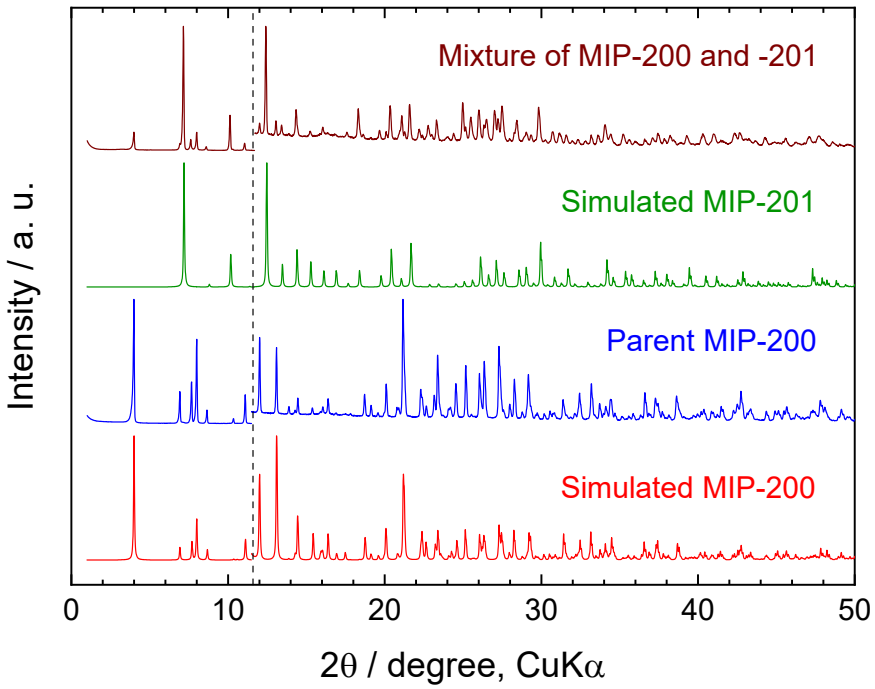

Figure S5 Comparison of XRPD patterns of the parent MIP-200 with those calculated from the corresponding CIF files for MIP-200 (labelled as simulated MIP-200)[5] and MIP-201 (labelled as simulated MIP-201)[19]. The pattern labelled as mixture of MIP-200 and MIP-201 belongs to the sample containing both phases synthesized according to the original procedure.[5] Diffractograms are normalized and shifted vertically to avoid overlaps. The diffractograms are zoomed from 11.75° 2θ to visualize diffractions at higher angles.

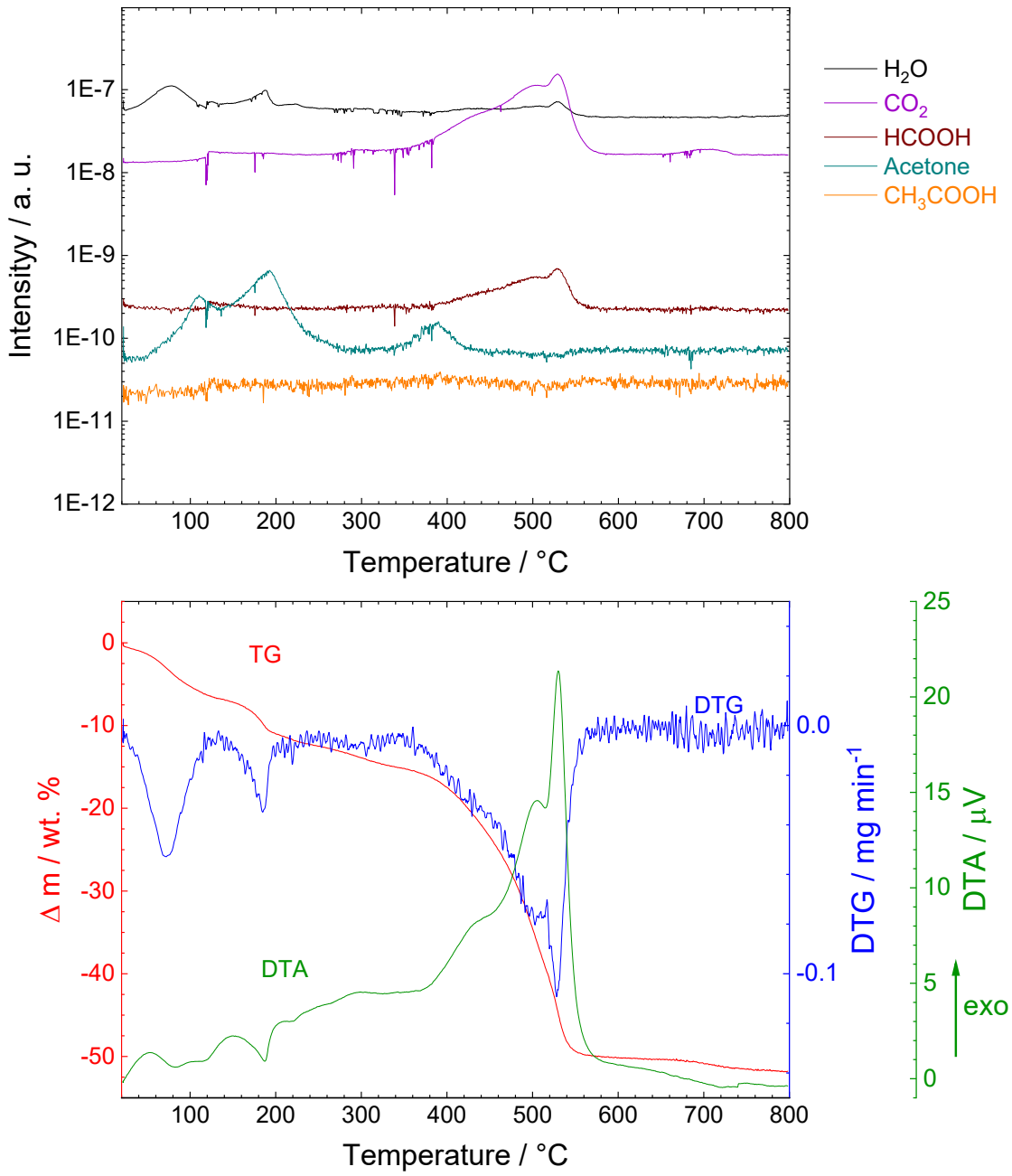

Figure S6 TGA/DTA curves of the parent MIP-200 (bottom) and MS analysis of the gases evolved during the TGA measurement (top).

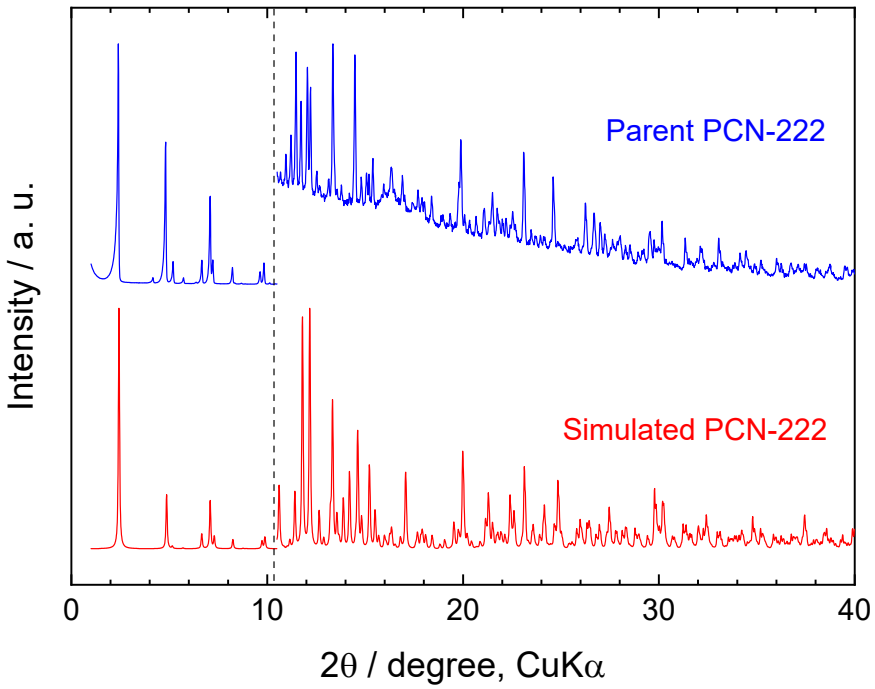

Figure S7 XRPD pattern of the parent PCN-222 compared with that calculated from the corresponding CIF file.[20] Diffractograms are normalized and shifted vertically to avoid overlaps. The diffractograms are zoomed from 10.5° 2θ to visualize diffractions at higher angles.

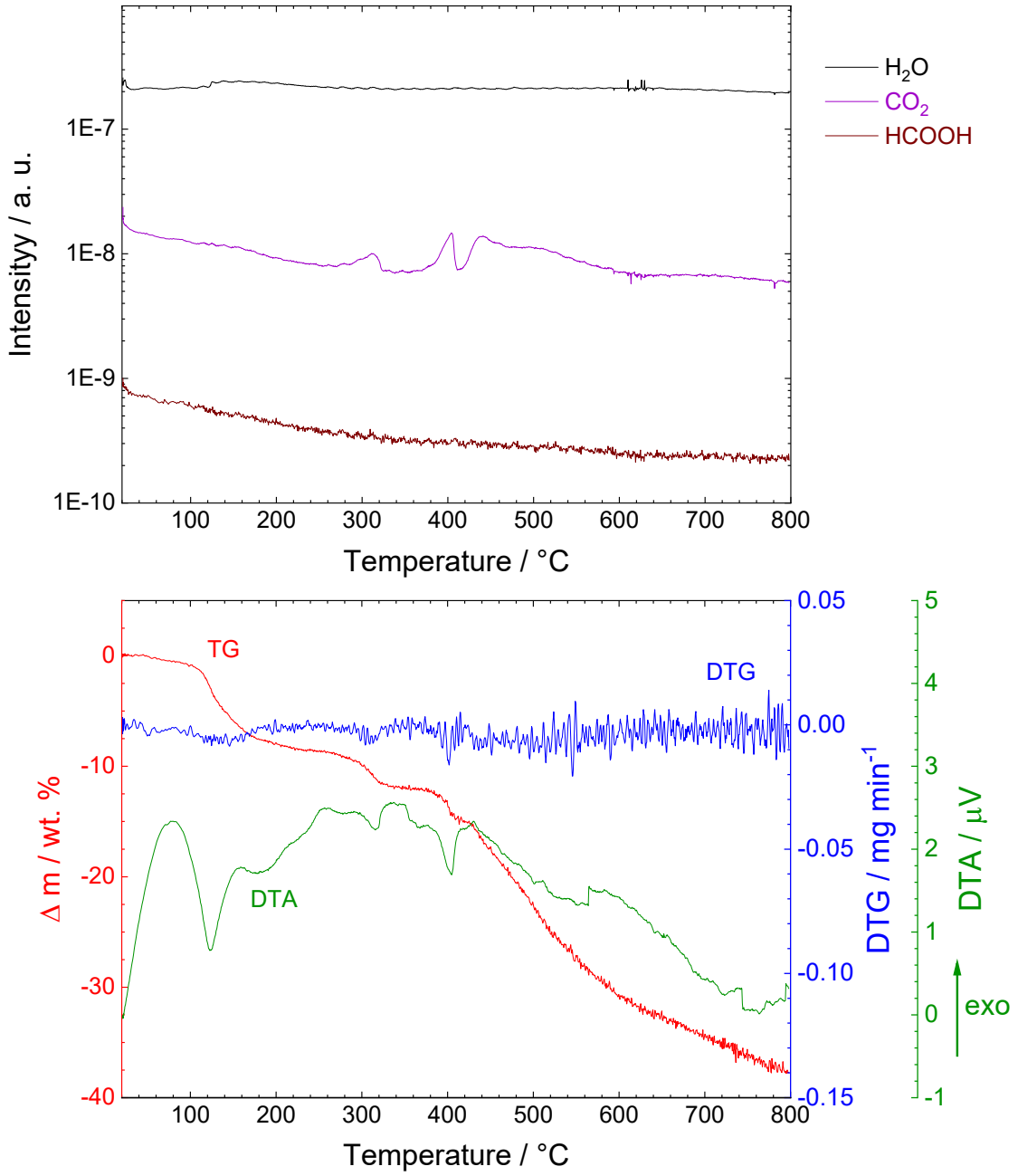

Figure S8 TGA/DTA curves of the parent PCN-222 (bottom) and MS analysis of the gases evolved during the TGA measurement (top).

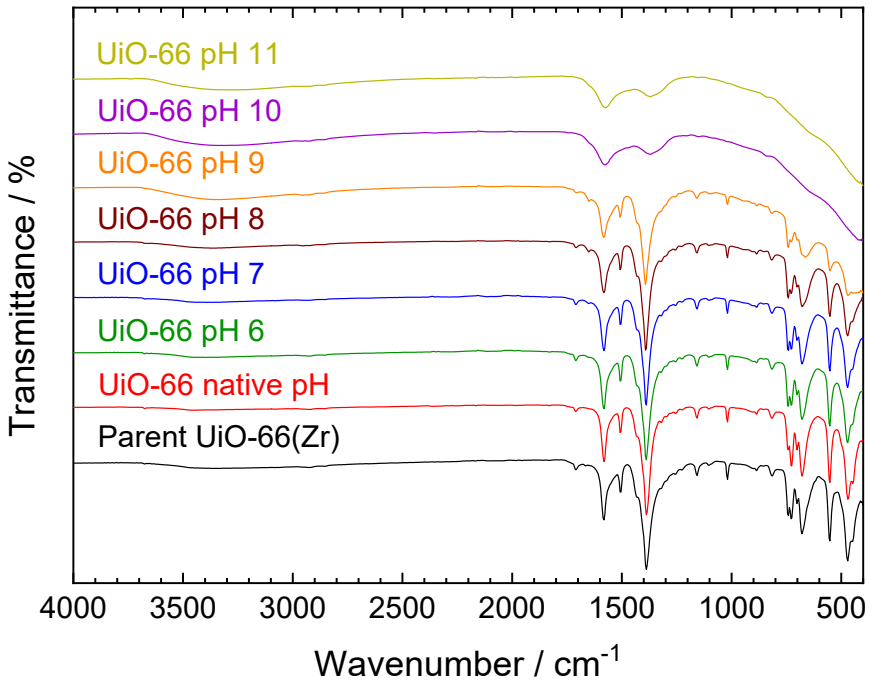

Figure S9 FTIR spectra of the parent and post-exposure UiO-66. Spectra are normalized and shifted vertically to avoid overlaps.

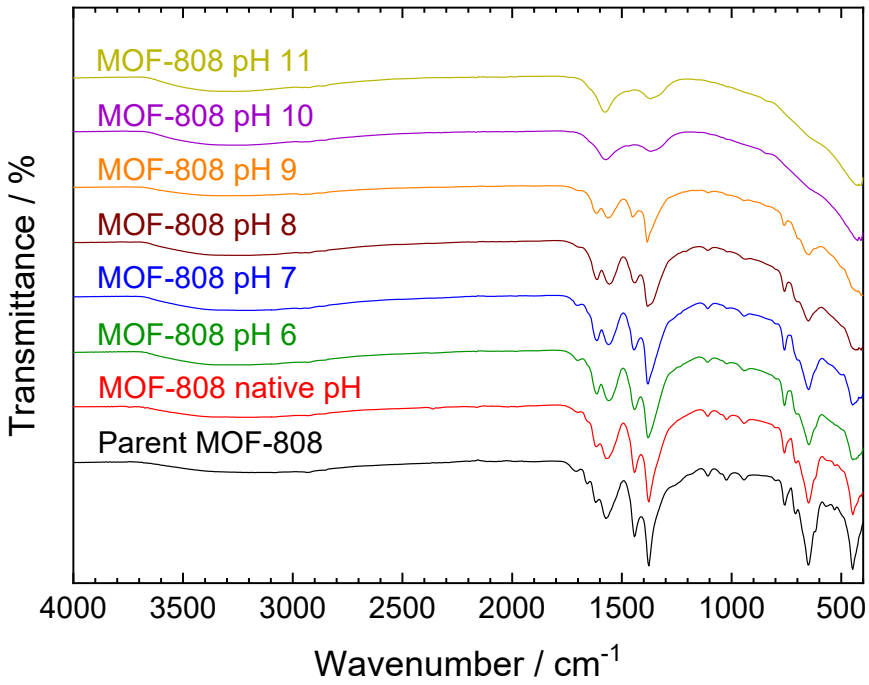

Figure S10 FTIR spectra of the parent and post-exposure MOF-808. Spectra are normalized and shifted vertically to avoid overlaps.

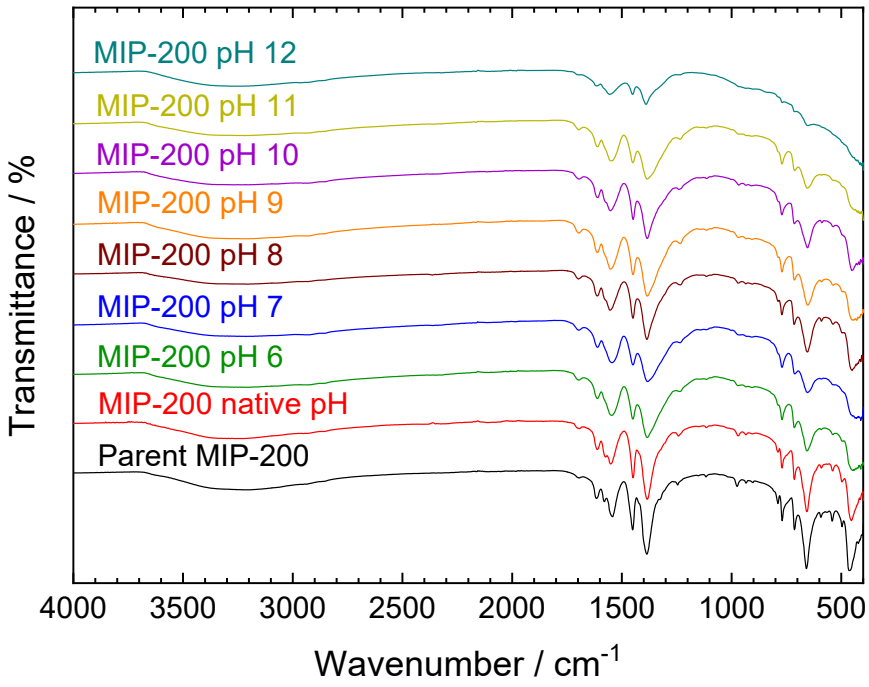

Figure S11 FTIR spectra of the parent and post-exposure MIP-200. Spectra are normalized and shifted vertically to avoid overlaps.

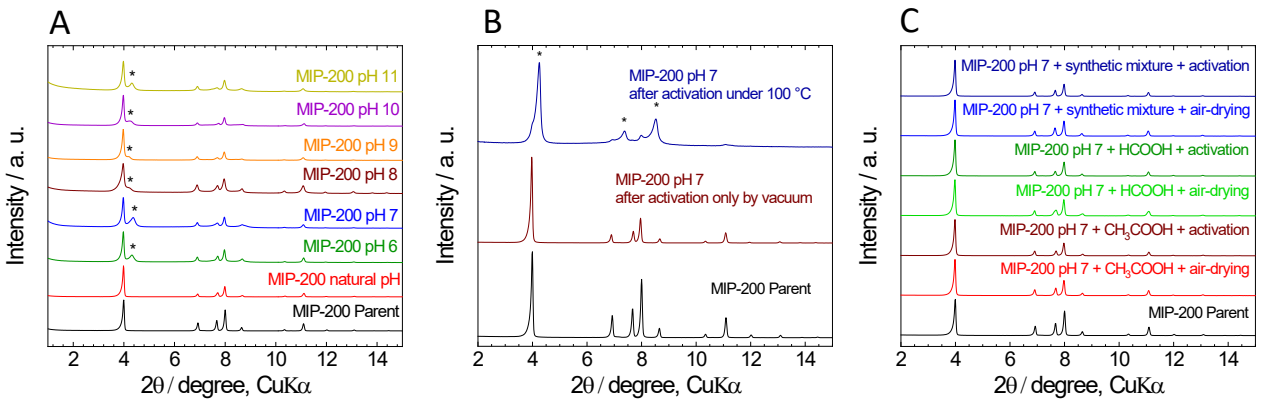

Figure S12 A. XRPD patterns of parent and post-exposure MIP-200 at a given pH after their reactivation at 100 °C in air. B. XRPD pattern of parent MIP-200 compared with those of MIP-200 treated at pH 7.0 for 4 h followed by overnight reactivation by evacuation at room temperature (brown) and reactivation at 100 °C in air (blue). C. XRPD patterns of MIP-200 after treatment at pH 7.0 for 4 h, which was then treated with acetic acid, formic acid, and a mixture of acetic anhydride with formic acid (mixture used for MIP-200 crystallization), XRPD patterns were measured before (air-drying) and after reactivation at 100 °C in air overnight. The diffractions of a new phase are indicated by *. The diffractograms are normalized and shifted vertically to avoid overlaps.

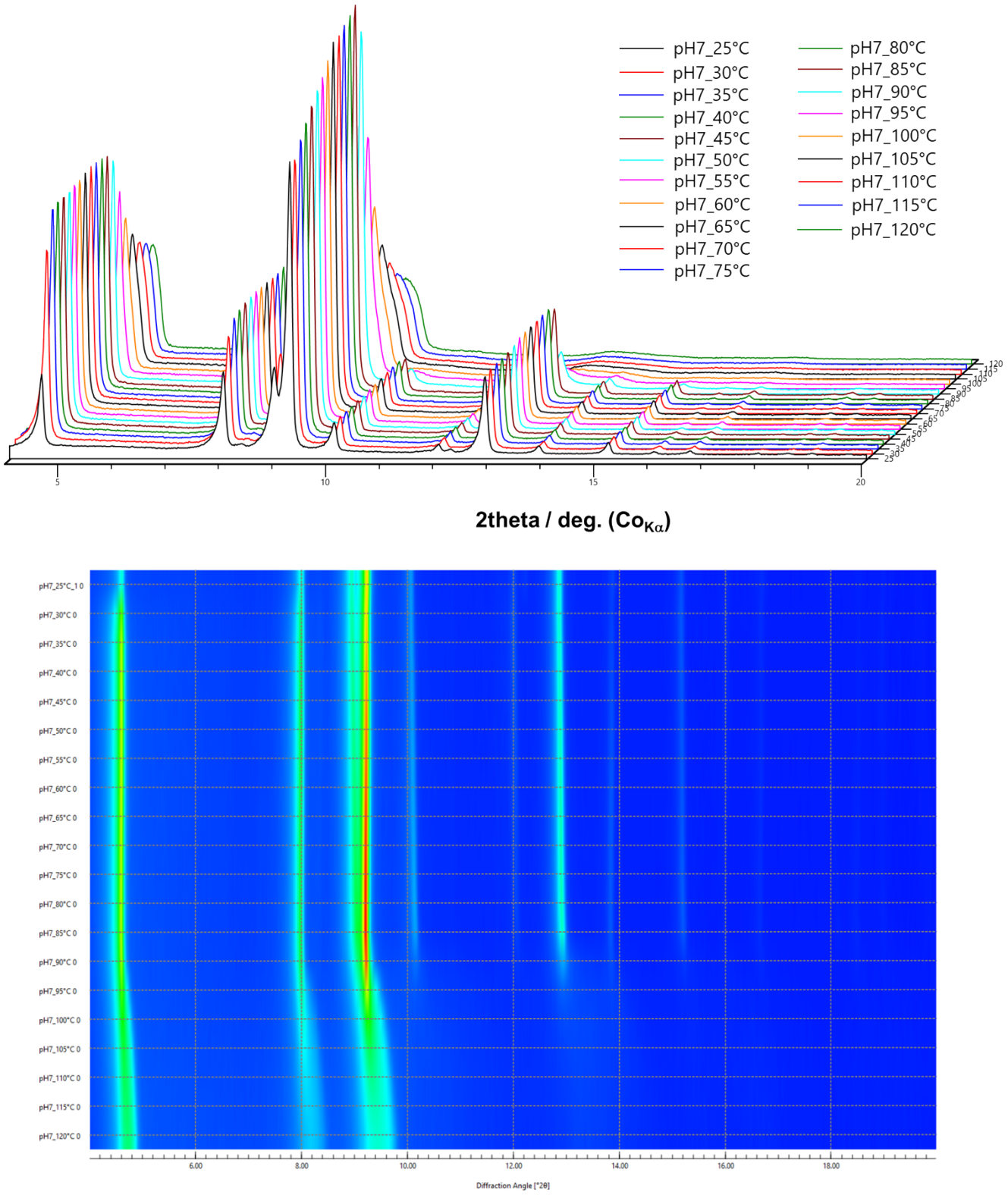

Figure S13 Temperature dependent PXRD patterns of MIP-200 treated at pH 7.0 (top) and 3D map of diffractions (bottom).

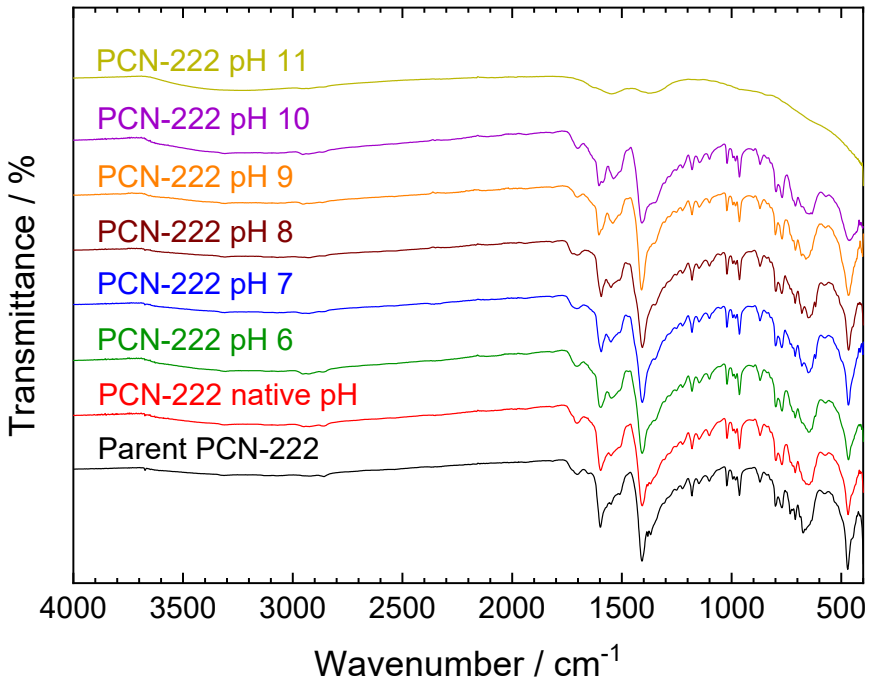

Figure S14 FTIR spectra of the parent and post-exposure PCN-222. Spectra are normalized and shifted vertically to avoid overlaps.

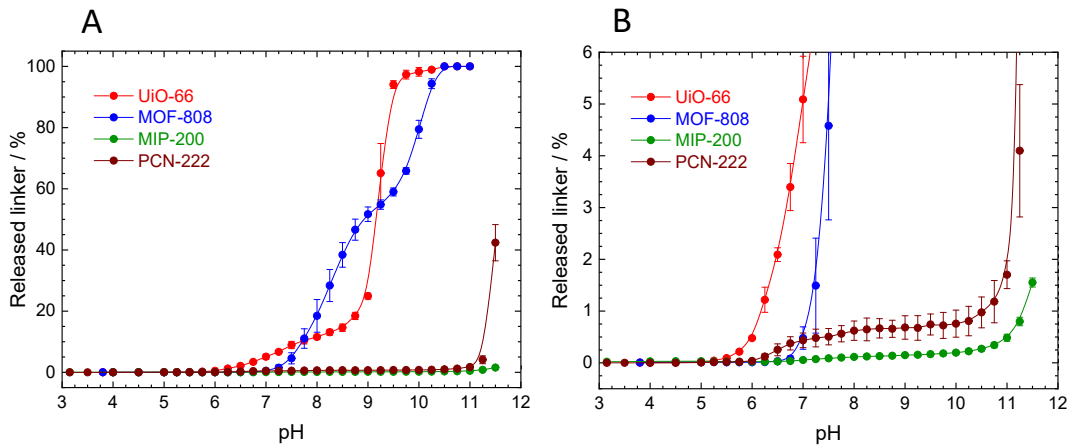

Figure S15 Comparison of immediate linker release from the MOFs. A. complete view; B. zoomed in area below 6 % to make the low amounts of linker release more visible.

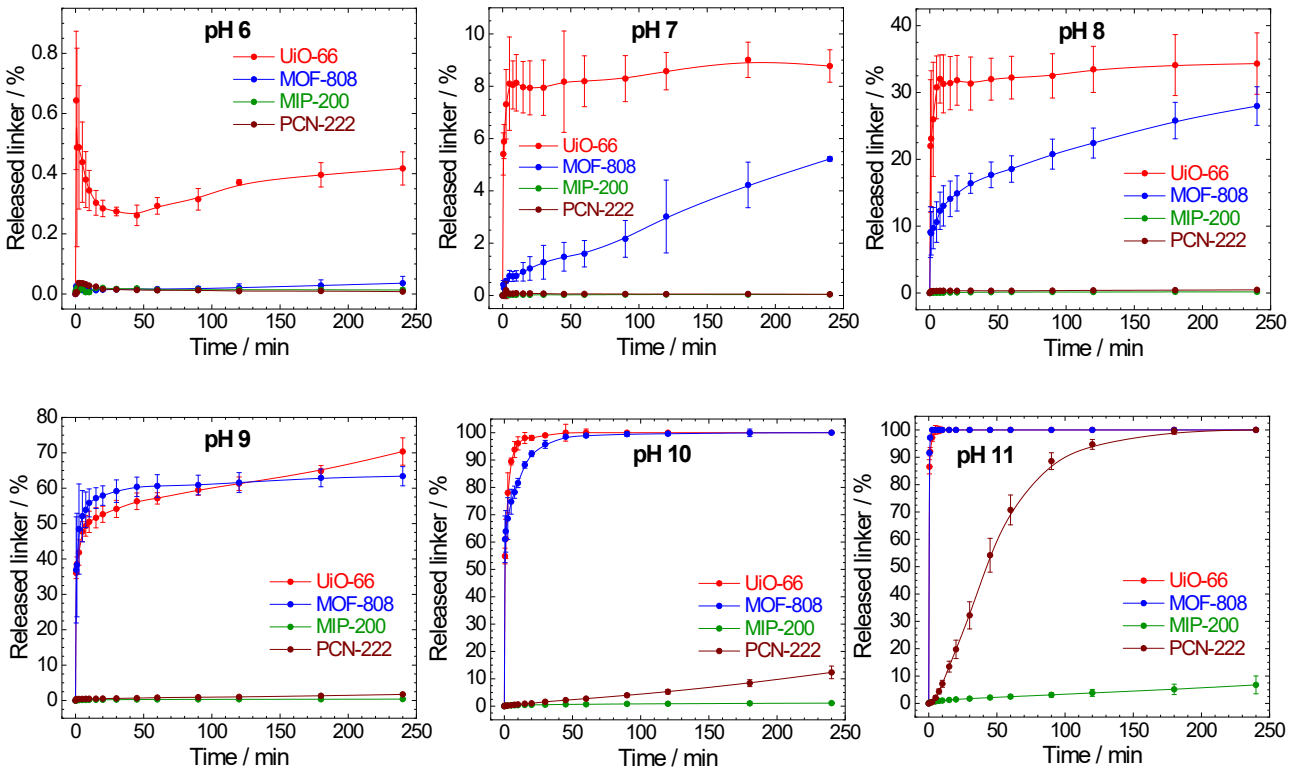

Figure S16 Comparison of the time-dependent linker release at given pH values.

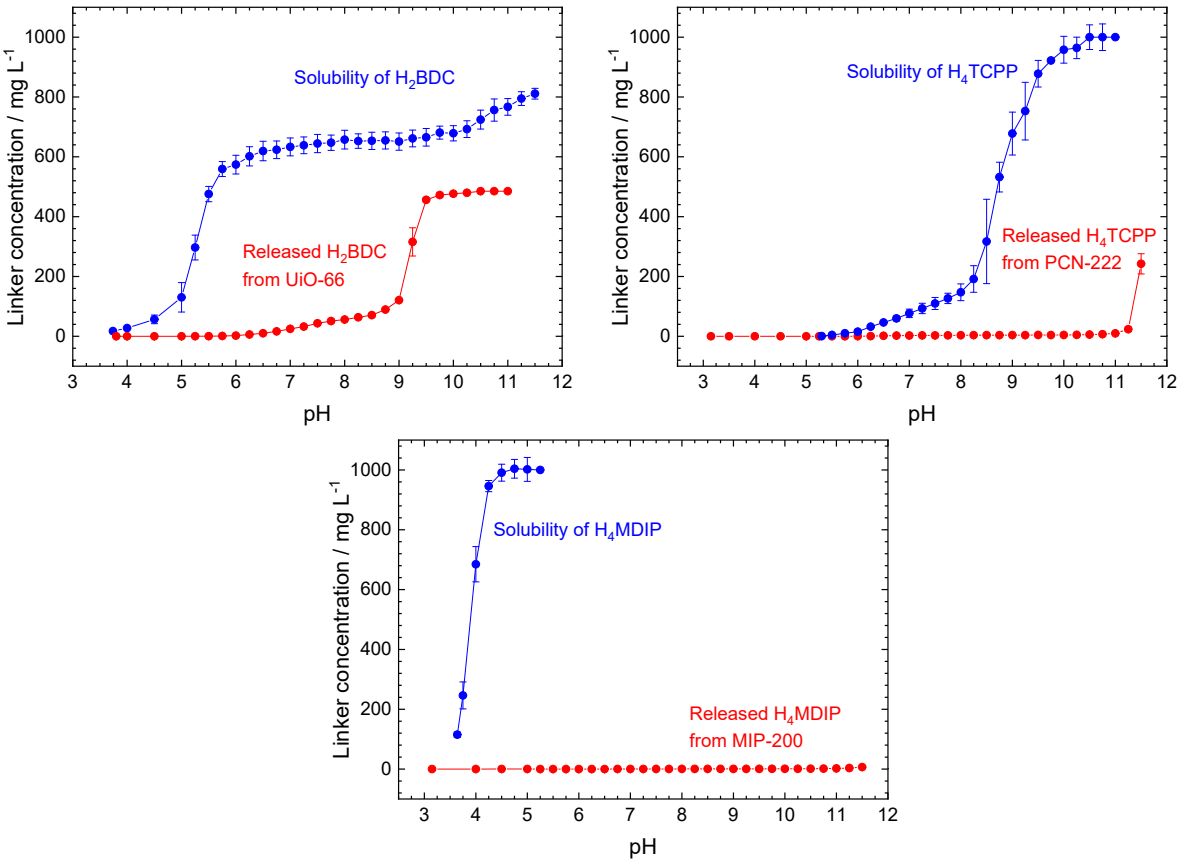

Figure S17 Comparison of immediate linker release from given MOFs and solubility of the linkers during the titration experiment. The maximum concentration which can be detected in the present setup was 1000 mg L^{-1}, for this reason the higher concentrations are not included. MOF-808 is not included in the figure because H_3BTC is well soluble in neat water without pH adjustment (up to 1000 mg L^{-1}).

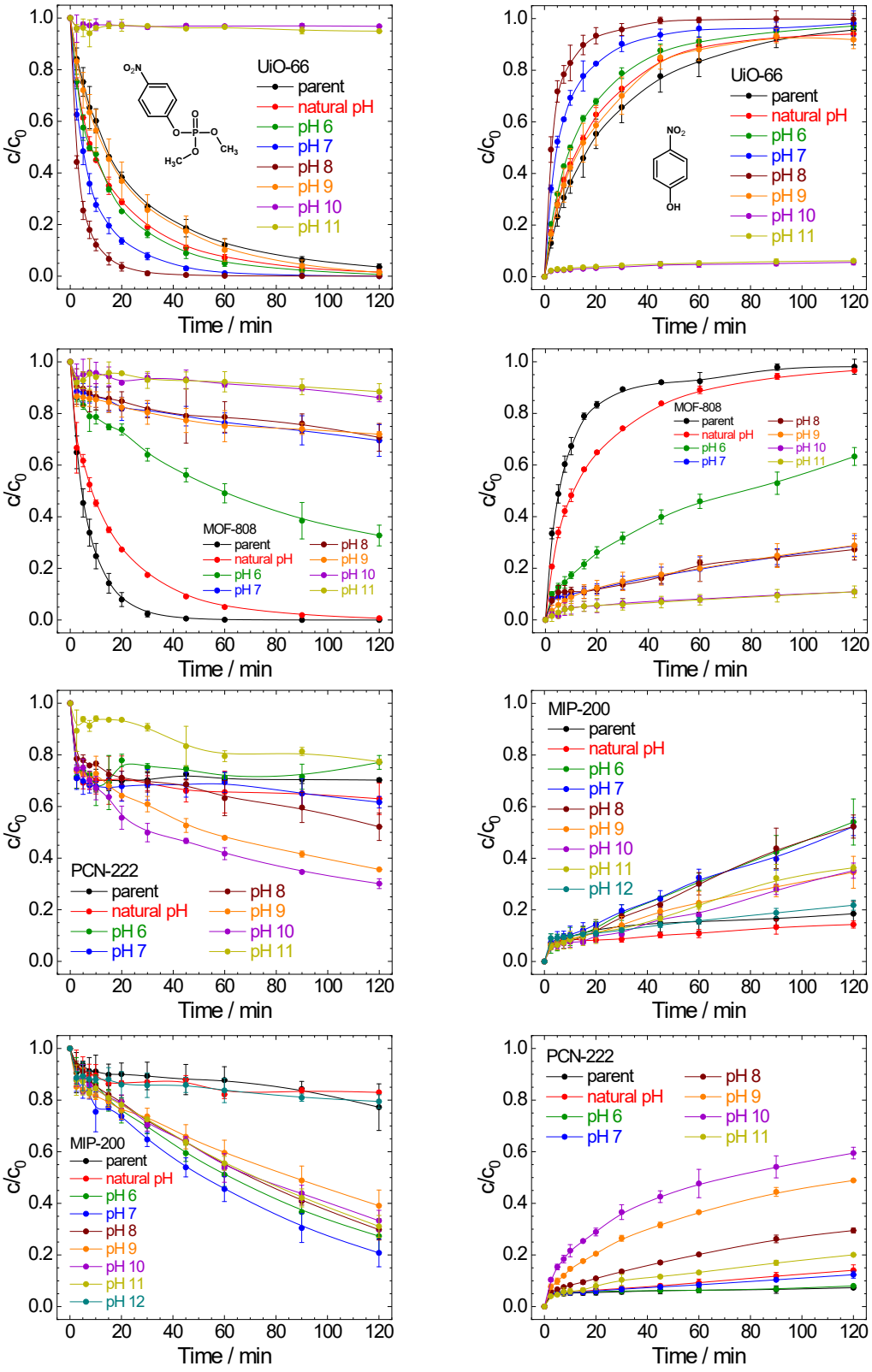

Figure S18 Kinetic profiles of DMNP degradation (left column) and 4-NP production (right column).

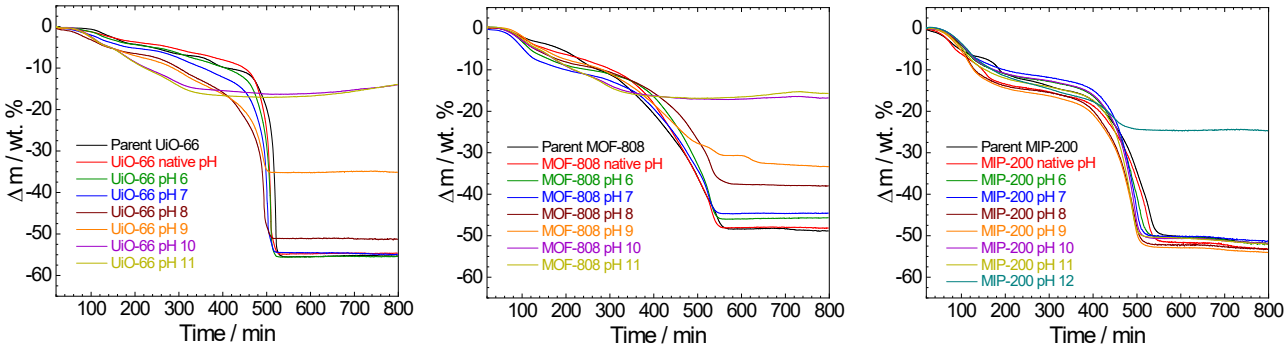

Figure S19 TGA curves of the parent and post-exposure UiO-66 (left), MOF-808 (middle), and MIP-200 (right).

Table S3 Content of BDC^{2-}, Zr, and monocarboxylate ligands (formate and acetate) in the parent UiO-66 and UiO-66 after the treatment for 240 min at different pHs, including the percentage of BDC^{2-} released from the MOF structure after the 240 min treatment with respect to the parent UiO-66 and total TGA mass loss. Molar ratios of all components are summarized in Table S4. Corresponding TGA curves are given in Figure S19.

Sample	Zr / wt%	BDC^{2-} / wt%	Formate / wt%	Acetate / wt%	BDC^{2-} release / %	TGA mass decrease wt%
UiO-66 parent	30.1 ± 0.2	48.5 ± 2.4	1.23 ± 0.01	1.10 ± 0.09	0.0	55.3
UiO-66 pH nat.[a]	27.2 ± 1.2	45.7 ± 3.3	1.06 ± 0.07	<LOD	<LOD	54.6
UiO-66 pH 6	31.3 ± 0.3	45.5 ± 2.6	1.70 ± 0.17	<LOD	0.4 ± 0.1	55.4
UiO-66 pH 7	32.0 ± 0.7	45.1 ± 4.4	0.99 ± 0.05	<LOD	8.8 ± 0.6	54.7
UiO-66 pH 8	33.2 ± 0.1	34.6 ± 3.7	1.24 ± 0.01	<LOD	34.3 ± 4.6	51.1
UiO-66 pH 9	46.4 ± 1.3	21.3 ± 1.1	1.64 ± 0.26	<LOD	70.4 ± 3.9	35.0
UiO-66 pH 10	60.7 ± 1.1	0.6 ± 0.4	4.34 ± 0.02	<LOD	100	14.9
UiO-66 pH 11	59.0 ± 0.4	<LOD	4.79 ± 0.07	<LOD	100	15.1

[a] Natural pH is 3.8

Table S4 Molar ratios of BDC^{2-}, Zr, and monocarboxylate ligands (formate and acetate) in the parent and treated UiO-66. The molar content is given as ratio to Zr_6 cluster.

Sample	Zr / mol	BDC^{2-} / mol	Formate / mol	Acetate / mol
UiO-66 parent	6	5.31	0.49	0.33
UiO-66 pH nat.[a]	6	5.54	0.47	0
UiO-66 pH 6	6	4.79	0.65	0
UiO-66 pH 7	6	4.64	0.37	0
UiO-66 pH 8	6	3.43	0.44	0
UiO-66 pH 9	6	1.51	0.42	0
UiO-66 pH 10	6	0.03	0.85	0
UiO-66 pH 11	6	0	0.97	0

[a] Natural pH is 3.8

Table S5 Content of BTC^{3-}, Zr, and monocarboxylate ligands (formate and acetate) in the parent MOF-808 and MOF-808 after the treatment for 240 min at different pHs, including the percentage of BTC^{3-} released from the MOF structure after the 240 min treatment with respect to the parent MOF-808 and total TGA mass loss. Molar ratios of all components are summarized in Table S6. Corresponding TGA curves are given in Figure S19.

Sample	Zr / wt%	BTC^{3-} / wt%	Formate / wt%	Acetate / wt%	BTC^{3-} release / %	TGA mass decrease wt%
MOF-808 parent	34.8 ± 2.8	28.2 ± 4.5	8.04 ± 0.60	26.99 ± 2.28	n.a.	48.8
MOF-808 pH nat.[a]	34.1 ± 2.4	29.5 ± 2.5	5.71 ± 0.44	17.98 ± 0.70	<LOD	48.2
MOF-808 pH 6	34.5 ± 0.9	30.4 ± 0.3	3.38 ± 0.54	7.15 ± 1.47	0.04 ± 0.02	45.7
MOF-808 pH 7	35.8 ± 4.8	29.4 ± 2.5	4.26 ± 1.12	1.32 ± 1.29	5.2 ± 0.1	44.5
MOF-808 pH 8	39.5 ± 3.5	25.1 ± 2.3	5.20 ± 1.59	<LOD	27.9 ± 2.8	38.0
MOF-808 pH 9	46.6 ± 5.3	13.7 ± 3.3	6.52 ± 2.23	<LOD	63.4 ± 2.7	33.3
MOF-808 pH 10	53.7 ± 3.2	0.9 ± 0.2	6.09 ± 0.18	0.39 ± 0.06	100	16.8
MOF-808 pH 11	50.9 ± 3.3	0.1 ± 0.1	9.37 ± 0.71	0.23 ± 0.15	100	15.9

[a] Natural pH is 3.8

Table S6 Molar ratios of BTC^{3-}, Zr, and monocarboxylate ligands (formate and acetate) in the parent and treated MOF-808. The molar content is given as ratio to Zr_6 cluster.

Sample	Zr / mol	BTC^{3-} / mol	Formate / mol	Acetate / mol
MOF-808 parent	6	2.12	2.75	7.07
MOF-808 pH nat.[a]	6	2.52	1.99	4.54
MOF-808 pH 6	6	2.30	1.17	1.89
MOF-808 pH 7	6	2.14	1.42	0.33
MOF-808 pH 8	6	1.65	1.57	0
MOF-808 pH 9	6	0.76	1.66	0
MOF-808 pH 10	6	0.04	1.35	0.07
MOF-808 pH 11	6	0.01	2.19	0.04

[a] Natural pH is 3.8

Table S7 Content of $MDIP^{4-}$, Zr, and monocarboxylate ligands (formate and acetate) in the parent MIP-200 and MIP-200 after the treatment for 240 min at different pHs, including the percentage of $MDIP^{4-}$ released from the MOF structure after the 240 min treatment with respect to the parent MIP-200 and total TGA mass loss. Molar ratios of all components are summarized in Table S8. Corresponding TGA curves are given in Figure S19.

Sample	Zr / wt%	$MDIP^{4-}$ / wt%	Formate / wt%	Acetate / wt%	$MDIP^{4-}$ release / %	TGA mass decrease wt%
MIP-200 parent	29.0 ± 1.1	42.1 ± 5.9	1.74 ± 0.01	0.52 ± 0.01	n.a.	51.9
MIP-200 pH nat.[a]	30.2 ± 0.7	41.5 ± 2.6	1.49 ± 0.08	0.05 ± 0.01	<LOD	53.3
MIP-200 pH 6	31.6 ± 0.5	43.5 ± 1.7	0.69 ± 0.06	<LOD	0.01 ± 0.007	52.0
MIP-200 pH 7	32.5 ± 1.6	44.8 ± 0.3	0.43 ± 0.03	<LOD	0.04 ± 0.03	51.3
MIP-200 pH 8	31.1 ± 0.3	43.1 ± 2.1	0.38 ± 0.07	<LOD	0.17 ± 0.07	53.3
MIP-200 pH 9	30.4 ± 0.6	42.3 ± 0.6	0.29 ± 0.08	<LOD	0.40 ± 0.25	54.1
MIP-200 pH 10	32.7 ± 0.1	43.9 ± 0.3	0.29 ± 0.02	<LOD	1.11 ± 0.56	51.8
MIP-200 pH 11	32.2 ± 1.7	41.6 ± 0.8	0.35 ± 0.07	<LOD	6.77 ± 3.26	52.0
MIP-200 pH 12	49.7 ± 1.0	2.8 ± 0.8	<LOD	<LOD	85.34 ± 3.17	24.8

[a] Natural pH is 3.2.

Table S8 Molar ratios of $MDIP^{4-}$, Zr, and monocarboxylate ligands (formate and acetate) in the parent and treated MIP-200. The molar content is given as ratio to Zr_6 cluster.

MOF	Zr / mol	$MDIP^{4-}$ / mol	Formate / mol	Acetate / mol
MIP-200 parent	6	2.31	0.71	0.16
MIP-200 pH nat.[a]	6	2.18	0.59	0
MIP-200 pH 6	6	2.19	0.26	0
MIP-200 pH 7	6	2.19	0.16	0
MIP-200 pH 8	6	2.20	0.15	0
MIP-200 pH 9	6	2.21	0.12	0
MIP-200 pH 10	6	2.13	0.10	0
MIP-200 pH 11	6	2.05	0.13	0
MIP-200 pH 12	6	0.09	0.04	0

[a] Natural pH is 3.2.

Table S9 Content of $TCPP^{4-}$, Zr, and monocarboxylate ligands (formate and acetate) in the parent PCN-222 and PCN-222 after the treatment for 240 min at different pHs, including the percentage of $TCPP^{4-}$ released from the MOF structure after the 240 min treatment with respect to the parent PCN-222 and total TGA mass loss. Molar ratios of all components are summarized in Table S10.

Sample	Zr / wt%	$TCPP^{4-}$ / wt%	Formate / wt%	Acetate / wt%	$TCPP^{4-}$ release / %
PCN-222 parent	19.0 ± 0.5	59.8 ± 1.7	7.1 ± 0.4	<LOD	0
PCN-222 pH nat.[a]	17.6 ± 0.4	60.6 ± 0.3	3.4 ± 0.2	<LOD	<LOD
PCN-222 pH 6	19.1 ± 0.3	64.1 ± 0.3	0.3 ± 0.1	<LOD	0.008 ± 0.001
PCN-222 pH 7	17.8 ± 0.1	60.1 ± 0.8	0.5 ± 0.1	<LOD	0.04 ± 0.02
PCN-222 pH 8	17.4 ± 0.6	56.6 ± 0.7	0.7 ± 0.1	<LOD	0.48 ± 0.03
PCN-222 pH 9	17.6 ± 0.3	60.3 ± 1.0	0.5 ± 0.2	<LOD	1.73 ± 0.27
PCN-222 pH 10	19.0 ± 0.2	59.1 ± 0.7	0.3 ± 0.1	<LOD	12.34 ± 2.30
PCN-222 pH 11	56.7 ± 0.9	1.7 ± 0.4	0.3 ± 0.1	<LOD	100

[a] Natural pH is 3.2.

Table S10 Molar ratios of $TCPP^{4-}$, Zr, and monocarboxylate ligands (formate and acetate) in the parent and treated PCN-222. The molar content is given as ratio to Zr_6 cluster.

Sample	Zr / mol	$TCPP^{4-}$ / mol	Formate / mol	Acetate / mol
PCN-222 parent	6	2.17	4.41	0
PCN-222 pH nat.[a]	6	2.38	2.31	0
PCN-222 pH 6	6	2.25	0.48	0
PCN-222 pH 7	6	2.34	0.32	0
PCN-222 pH 8	6	2.32	0.18	0
PCN-222 pH 9	6	2.37	0.32	0
PCN-222 pH 10	6	2.15	0.19	0
PCN-222 pH 11	6	0.02	0.05	0

[a] Natural pH is 3.2.

Table S11 Calculated amorphous content in the parent and post-exposure UiO-66.

Sample	Crystalline phase / %	Amorph / %	a / Å[a]	D / nm[b]	Rwp[c]
UiO-66 parent	74.2±0.5	25.8±0.5	20.7798±0.0001	433.0±14.0	9.28
UiO-66 pH nat.[d]	64.2±0.5	35.8±0.5	20.7740±0.0002	206.7±4.5	9.8
UiO-66 pH 6	62.1±0.5	37.9±0.5	20.7639±0.0002	167.1±3.1	9.43
UiO-66 pH 7	60.8±0.5	39.2±0.5	20.7740±0.0002	172.8±2.8	9.8
UiO-66 pH 8	48.9±0.4	51.1±0.4	20.7633±0.0003	189.7±4.2	8.57
UiO-66 pH 9	27.2±0.2	72.8±0.2	20.7482±0.0005	161.1±3.6	5.94
UiO-66 pH 10	0	100			
UiO-66 pH 11	0	100			

[a] Unit cell parameter
[b] Mean crystallite size
[c] Agreement factor
[d] Natural pH is 3.8

Table S12 Influence of grinding MOFs with ZnO on the content of crystalline phase.

Sample	Grinding	Crystalline phase / %	Amorph / %	Rwp[a]
UiO-66 Parent	1st	67.8±0.5	32.2±0.5	9.56
	2nd	65.7±0.5	34.3±0.5	9.48
	3rd	65.3±0.5	34.7±0.5	9.07
MOF-808 Parent	1st	31.2±0.3	68.8±0.3	10.44
	2nd	26.1±0.3	74.0±0.3	8.07
	3rd	24.0±0.3	76.0±0.3	8.03
MIP-200 Parent	1st	11.3±0.2	88.7±0.2	17.2
	2nd	12.0±0.2	88.0±0.2	15.8
	3rd	11.8±0.2	88.2±0.2	13.96
PCN-222 Parent	1st	8.2±0.2	91.8±0.2	15.58
	2nd	7.8±0.2	92.3±0.2	12.56
	3rd	6.2±0.2	93.8±0.2	14.25

[a] Unit cell parameter

Table S13 Calculated amorphous content in the parent and post-exposure MIP-200.

Sample	Crystalline phase / %	Amorph / %	a / Å[a]	D / nm[b]	Rwp[c]
MIP-200 parent[d]	12.8±0.2	87.2±0.2	25.5109±0.0013	11.6154±0.0014	172.0±11.0
MIP-200 nat.[e]	14.4±0.2	85.6±0.2	25.5921±0.0015	11.5834±0.0015	134.5±6.9
MIP-200 pH 6	13.4±0.2	86.6±0.2	25.6185±0.0016	11.4763±0.0017	106.6±4.5
MIP-200 pH 7	13.4±0.2	86.6±0.2	25.6285±0.0016	11.4756±0.0015	122.5±5.4
MIP-200 pH 8	13.0±0.2	87.0±0.2	25.6411±0.0014	11.5072±0.0015	128.0±6.0
MIP-200 pH 9	13.4±0.2	86.6±0.2	25.6402±0.0015	11.5167±0.0015	120.8±5.5
MIP-200 pH 10	12.9±0.2	87.1±0.2	25.6400±0.0015	11.5070±0.0014	132.2±6.2
MIP-200 pH 11	12.1±0.2	87.9±0.2	25.6393±0.0014	11.5036±0.0016	134.3±6.7
MIP-200 pH 12	3.3±0.3	96.7±0.3	25.5976±0.0032	11.3652±0.0010	11.4±0.8

[a] Unit cell parameter
[b] Mean crystallite size
[c] Agreement factor
[d] In the case of MIP-200, the estimation of the crystalline and amorphous phase content was not sufficiently precise because the only existing structure model does not fit our experimental data well, and there are doubts about its applicability to our samples. This could be one of the reasons why such a high amorphous content was detected in the parent MIP-200.
[e] Natural pH is 3.2

References

[1] J. H. Cavka, S. Jakobsen, U. Olsbye, N. Guillou, C. Lamberti, S. Bordiga, K. P, Lillerud, A New Zirconium Inorganic Building Brick Forming Metal Organic Frameworks with Exceptional Stability, *J. Am. Chem. Soc.*, 2008, **130**, 42, 13850-13851.

[2] D. Bůžek, S. Adamec, K. Lang, J. Demel, Metal–organic frameworks vs. buffers: case study of UiO-66 stability, *Inorg. Chem. Front.*, 2021, **8**, 720-734.

[3] M. Lammert, M. T. Wharmby, S. Smolders, B. Bueken, A. Lieb, K. A. Lomachenko, D. De Vos, N. Stock, Cerium-based metal organic frameworks with UiO-66 architecture: synthesis, properties and redox catalytic activity, *Chem. Commun.*, 2015, **51**, 12578-12581.

[4] J. Xu, J. Liu, Z. Li, X. Wang, Y. Xu, S. Chen, Z. Wang, Optimized synthesis of Zr(iv) metal organic frameworks (MOFs-808) for efficient hydrogen storage, *New J. Chem.*, 2019, **43**, 4092-4099.

[5] S. Wang, J. S. Lee, M. Wahiduzzaman, J. Park, M. Muschi, C. Martineau-Corcos, A. Tissot, K. H. Cho, J. Marrot, W. Shepard, G. Maurin, J.-S. Chang, C. Serre, A robust large-pore zirconium carboxylate metal–organic framework for energy-efficient water-sorption-driven refrigeration, *Nature Energy*, 2018, **3**, 985-993.

[6] A. K. Yetisen, M. M. Qasim, S. Nosheen, T. D. Wilkinson, C. R. Lowe, Pulsed laser writing of holographic nanosensors, *J. Mater. Chem*., 2014, **2** , 3569-3576

[7] D. Bůžek, J. Zelenka, P. Ulbrich, T. Ruml, I. Křížová, J. Lang, P. Kubát, J. Demel, K. Kirakci, K. Lang, Nanoscaled porphyrinic metal–organic frameworks: photosensitizer delivery systems for photodynamic therapy, *J. Mater. Chem. B*, 2017, **5**, 1815-1821.

[8] W. Morris, B. Volosskiy, S. Demir, F. Gándara, P. L. McGrier, H. Furukawa, D. Cascio, J. F. Stoddart, O. M. Yaghi, Synthesis, Structure, and Metalation of Two New Highly Porous Zirconium Metal–Organic Frameworks, *Inorg. Chem.*, 2012, **51**, 12, 6443-6445.

[9] T. Degen, M. Sadki, E., U. König and G. Nénert, The HighScore suite, *Powder Diffraction*, 2014, **29**, Suppl. S2, S13 - S18.

[10] S. Grazulis, D. Chateigner, R. T. Downs, A. T. Yokochi, M. Quiros, L. Lutterotti, E. Manakova, J. Butkus, P. Moeck, A. Le Bail, Crystallography Open Database – an open-access collection of crystal structures, *J. Appl. Cryst.*, 2009, **42**, 726-729.

[11] C. R. Groom, I. J. Bruno, M. P. Lightfoot, S. C. Ward, The Cambridge Structural Database, *Acta Cryst.*, 2016, **B72**, 171-179.

[12] ICDD (2023). PDF-5+ 2024. International Centre for Diffraction Data, Newtown Square, PA, USA

[13] J. Bergmann, P. Friedel, R. Kleeberg, BGMN – a new fundamental parameters based Rietveld program for laboratory X-ray sources, its use in quantitative analysis and structure investigations, *CPD Newsl. (Commission of Powder Diffraction, International Union of Crystallography)*, 1998, **20**, 5-8.

[14] J. Bergmann, T. Monecke, R. Kleeberg, Alternative algorithm for the correction of preferred orientation in Rietveld analysis, *J. Appl. Crystallogr.*, 2001, **34**, 16-19.

[15] N. Döbelin, R. Kleeberg, „Profex: a graphical user interface for the Rietveld refinement program BGMN„, *J. Appl. Crystallogr.*, 2015, **48**, 1573-1580.

[16] J. Bergmann, Rietveld Analysis Program BGMN, manual, 2005, 4th revised version, Dresden, Germany.

[17] S. Øien, D. Wragg, H. Reinsch, S. Svelle, S. Bordiga, C. Lamberti, K. P. Lillerud, Detailed Structure Analysis of Atomic Positions and Defects in Zirconium Metal–Organic Frameworks, *Cryst. Growth Des.*, 2014, **14**, 11, 5370-5372.

[18] H. Furukawa, F. Gándara, Y.-B. Zhang, J. Jiang, W. L. Queen, M. R. Hudson, O. M. Yaghi, Water Adsorption in Porous Metal–Organic Frameworks and Related Materials, *J. Am. Chem. Soc.*, 2014, **136**,

11, 4369-4381.
[19] S. Wang, H. G. T. Ly, M. Wahiduzzaman, C. Simms, I. Dovgaliuk, A. Tissot, G. Maurin, T. N. Parac-Vogt, C. Serre, A zirconium metal-organic framework with SOC topological net for catalytic peptide bond hydrolysis, *Nat Commun.*, 2022, **13**, 1284.
[20] D. Feng, Z.-Y. Gu, J.-R. Li, H.-L. Jiang, Z. Wei, P H.-C. Zhou, Zirconium-Metalloporphyrin PCN-222: Mesoporous Metal–Organic Frameworks with Ultrahigh Stability as Biomimetic Catalysts, *Angew. Chem. Int. Ed.*, 2012, **51**, 10307-10310.